

# Low resolution meets high: towards a resolution continuum from cells to atoms

Timothy S Baker\* and John E Johnson†

During the past five years, strategies have been developed for generating pseudo-atomic-resolution models of macromolecular complexes by combining the data from high-resolution structures of components with lower-resolution data for the entire complex.

## Addresses

\*Department of Biological Sciences, Purdue University, West Lafayette, IN 47907-1392, USA; e-mail: tsb@bragg.bio.purdue.edu

†Department of Molecular Biology, The Scripps Research Institute, 10550 North Torrey Pines Rd, La Jolla, CA 92037, USA; e-mail: jackj@scripps.edu

*Current Opinion in Structural Biology* 1996, 6:585–594

© Current Biology Ltd ISSN 0959-440X

## Abbreviations

<b>3D</b>	three-dimensional
<b>CTF</b>	contrast transfer function
<b>EM</b>	electron microscopy
<b>HRV</b>	human rhinovirus
<b>FHV</b>	Flock House virus
<b>TEM</b>	transmission electron microscopy (microscope)

## Introduction

Developments in modern biology have been judged on their ability to provide a quantitative description of the complex and coordinated chemical processes that define living systems. The goal in most of these efforts has been to develop detailed models that allow structure–function relationships to be recognized and tested with molecular genetics. By far the most successful approach in this area has been the reduction of complex processes into components that have been analyzed in great detail by high-resolution structural techniques and modern biochemical and biophysical methods. A few enzymes and some macromolecular complexes have been analyzed with sufficient resolution and insight that good agreement has been achieved between experiment and predictions based on chemical principals.

Although, in many cases, the ‘pieces’ are understood in detail, it has been known for decades that biological events are usually more than the sum of their parts. The area of structural cell biology, in which attempts are made to develop detailed models for megastructures, is emerging as a stimulating new domain for biophysics. Because it is unlikely that methods for directly imaging very large cellular complexes at atomic resolution will be available soon, the current challenge for structural cell biology is to establish the organization of the components of a complex biological process by combining data from a variety of biophysical methods. Such a synthesis requires

high-resolution structural methods (e.g. X-ray crystallography and NMR spectroscopy) to generate atomic models of the modules, and methods for imaging the whole complex, at lower resolution, such as cryo-electron microscopy (cryoEM) and three-dimensional (3D) image reconstruction to assemble them. The development of such an association can be likened to a 3D jigsaw puzzle, where pieces of known shapes and sizes are assembled within a defined border.

During the past five years, a number of valuable, pseudo-atomic model structures of macromolecular systems have been developed using this hybrid approach. In some cases, these structures have led to detailed chemical descriptions of biological phenomena. Reviews of such studies involving viruses [1–5] and actin–myosin complexes [6–9] provide a clear indication of the value of this approach. Critical assessments of the methods involved [10,11] and of the overall context of these techniques in structural biology [12] have also been published.

We will not attempt to review the literature here, but instead seek to provide a foundation for critical discussion. An extensive table that lists the methodologies used with the various biological systems is provided. We also identify key papers that describe the important milestones in this area, and others that represent recent contributions to the field.

The recent reports of projects that have utilized the combined methodologies can be fitted into two broad categories. ‘High resolution meets low’ is a comparative method wherein high-resolution structures or complexes are created from individual modules and imaged at lower resolution to validate the interpretation of a low-resolution structure. This approach may be subcategorized as qualitative, in which images of the model and observed structures are only presented for comparison by eye, and quantitative, in which a statistical comparison between the two structures is made. ‘Low resolution meets high’, on the other hand, refers to the approach in which high-resolution models are fitted to low-resolution density maps to derive pseudo-atomic resolution models. Table 1 categorizes the primary literature referenced herein by biological system and by method of resolution combination.

What are the criteria that define a successful marriage of structures derived at high and low resolution? First, the components of the complex structure should be placed in their proper relative positions within the envelope of

Table 1

## Macromolecules at low and high resolution.

Structure	Qualitative comparison*	Quantitative comparison*	Model fitting*	Pseudo model*
Chaperones	[50]			
Enzymes				
Catalase	[51]			
Glutamine synthetase				[52]
Gyrase B	[53]			
HIV-1 reverse transcriptase	[54]			
Protein kinase C	[55]			
Membrane-associated proteins				
Acetylcholine-Fab			[95]	
Annexin	[28,56]		[28,56]	
Bacteriorhodopsin				[57]
Cholera toxin	[58]			
F <sub>1</sub> -ATPase	[59]			
Influenza hemagglutinin	[60]			
Influenza hemagglutinin-Fab	[61]			
Light-harvesting complex II	[62*]		[62*]	
OmpF porin	[63*]		[63*]	
Photosystem II			[64]	
Proaerolysin	[65]		[65]	
Signal sequence binding protein SRP54		[66]	[66]	
Muscle and muscle-related proteins				
Acrosomal bundle	[67*]	[68,69]	[67*,68]	
Actin filament	[8,70-73]	[71]		
Actin-myosin filament	[70,71]	[35**,70,71]	[35**]	
Actin- $\alpha$ -actinin		[74]	[74]	
Actin-brush border myosin filament		[34**]	[34**]	
Actin-gelsolin filament		[75]	[75]	
Actin-tropomyosin thin filament			[76*]	
Actin-Fab			[77]	
Myosin filaments			[78]	
S1-decorated thin filament			[79]	
Tropomyosin				[80]
Respiratory proteins				
Hemocyanin		[81,82]		[81]
Hemocyanin-Fab		[83,84*]		[83]
Ribosome			[42,43,44*,45**,85]	
Streptavidin	[32**]			
Viruses				
Adenovirus			[3]	
Alphavirus	[39*]			
Alphavirus-Fab			[86*]	
Bacteriophage $\phi$ X174		[29*]	[29*]	
Cowpea chlorotic mottle virus	[30*]		[30*]	
Cowpea mosaic virus-Fab			[2,87,88]	
Cowpea mosaic virus-IgG			[87]	
Human rhinovirus-ICAM-1	[31]	[31,41,89]	[41,89]	
Human rhinovirus-2-Fab	[90**]		[90**]	
Human rhinovirus-14-Fab		[91**]	[4,38,92]	[91**]
Nodavirus	[31]	[5,24,31]		
Parvovirus-Fab	[27]	[31]	[27]	
Parvovirus-globoside receptor	[93*]	[93*]	[93*]	
Rotavirus	[94*]		[94*]	

\*Abbreviations: Qualitative comparison, qualitative comparison of EM density and X-ray structure; quantitative comparison, quantitative comparison of EM density and X-ray structure; model fitting, fit of atomic model to EM density map; pseudo model, build pseudo-atomic model of large structure.

the low-resolution structure, and they should be properly oriented so that the correct intermolecular interfaces are established in the model. The formation of a complex from isolated components may induce conformational changes in the component molecules. Second, large-scale

changes should be detectable in a low-resolution density distribution. The model building procedure generally can not directly determine small-scale changes in the polypeptide chain or side chains induced by associations, but an approximation to these movements may be

predicted by computational chemistry. Finally, the fidelity of such predicted fine structure must be tested by mutation studies of residues at the interface.

Although there are numerous ways to correlate and combine structural data from TEM with that from other methods (small- or large-angle X-ray or neutron scattering; X-ray fiber diffraction; etc.) at a variety of resolution levels, we shall focus strictly on studies in which high resolution structural information derived from X-ray crystallography has been combined with low-resolution information derived from transmission electron microscopy (TEM).

### Low-resolution density maps from transmission electron microscopy

For over 30 years TEM and image-reconstruction techniques have provided useful tools for exploring the structures of biological macromolecules ranging from small (<50 Å diameter) protein subunits up to large (>1000 Å) macromolecular complexes. TEM has provided important first glimpses of the structures of molecules that could not be crystallized in a form suitable for high-resolution diffraction studies or that were simply too large at the time to be studied by high-resolution diffraction or NMR spectroscopy techniques.

Until recently, most TEM structural studies have been performed with specimens encased in a thin layer of a negative stain, such as uranyl acetate. Negative stains dramatically enhance the contrast of otherwise 'invisible' biological molecules, and yield images that reveal the gross morphology of molecules and also the arrangement and disposition of subunits in oligomeric structures. However, because staining only reveals those surfaces of the specimen exposed to, and thereby contrasted with, stain molecules (5–8 Å diameter), the details of biological structures are typically visualized only at relatively low resolution (20–30 Å). With rare exceptions, it has not been possible to examine in proteins structural features such as  $\alpha$  helices or  $\beta$  sheets, which require resolutions exceeding 10 Å. Nonetheless, staining techniques are still widely used because negatively stained samples are relatively easy to prepare and the images obtained continue to provide valuable structural information.

The classic study by Henderson and Unwin [13] in 1975 of the purple membrane structure in three dimensions at 7 Å resolution marked a turning point in high-resolution biological TEM. In this and subsequent studies (e.g. [14–17]), the advent of methods to prepare and image unstained, hydrated biological samples made it possible, in principle, to study the native structure of any macromolecule at atomic or near-atomic resolution. Unstained, crystalline specimens are usually prepared by one of two methods: (a) they are embedded in a thin layer of a sugar (such as

glucose) and subsequently imaged in the microscope at room temperature or after being cooled to liquid-nitrogen temperature; or (b) they are vitrified in a thin layer of water at near liquid-nitrogen temperature and kept cold for cryomicroscopy (cryoTEM). This latter, 'frozen-hydrated', preparation technique has been the method of choice for examining unstained, non-crystalline specimens, though both procedures appear, on the basis of electron-diffraction measurements, to preserve the hydrated structure of biological specimens in the vacuum of the TEM to atomic resolution.

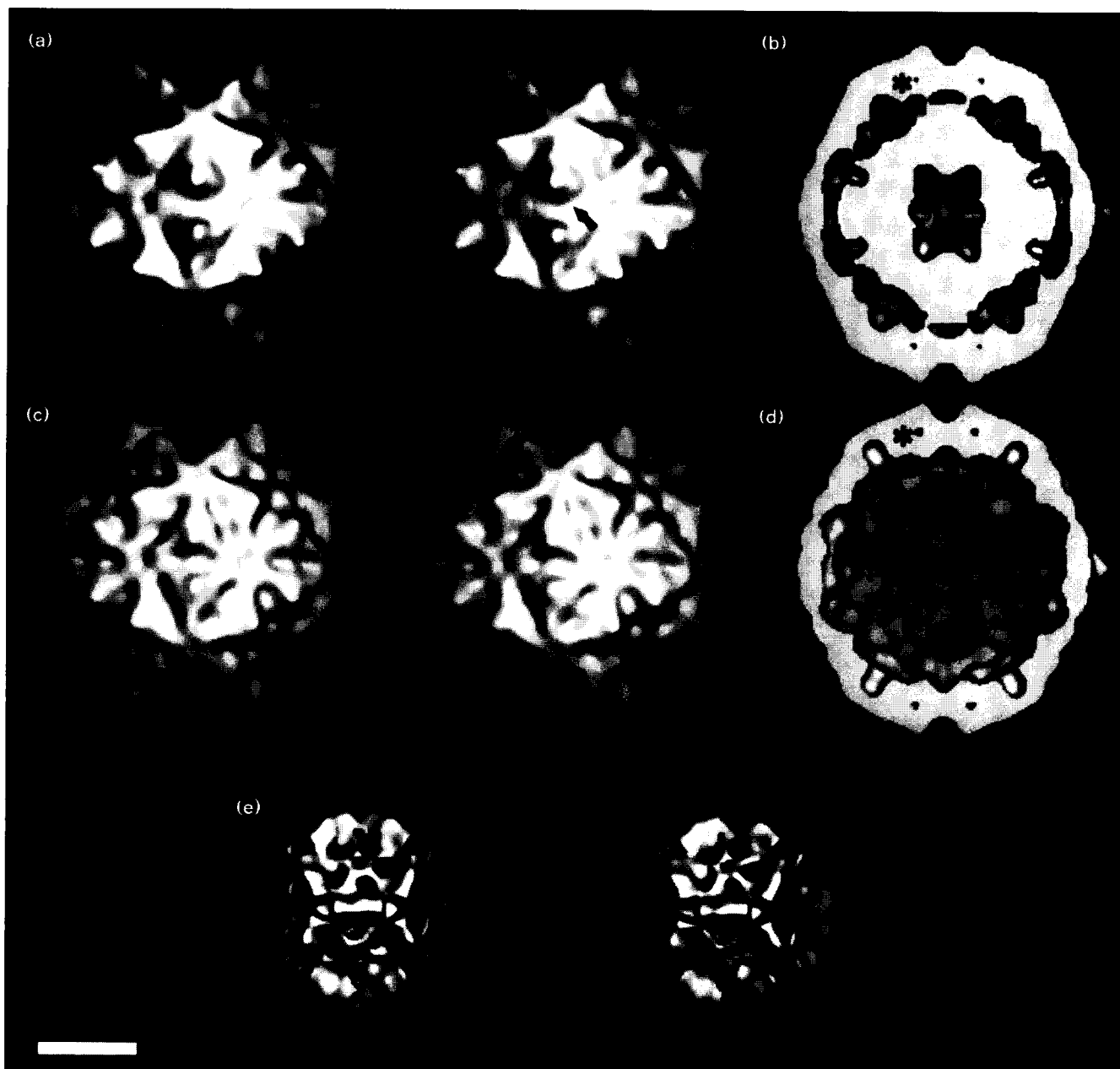
The low inherent contrast of unstained biological specimens and the high sensitivity of these specimens to the electron beam (1–5 electrons Å<sup>-2</sup> critical dose) necessitated the development of low-irradiation and defocus (phase-contrast) imaging procedures [13]. The resultant micrographs yield magnified specimen images that are quite noisy and are also 'distorted' by electron optical (e.g. chromatic and spherical aberration of the electromagnetic lenses; image astigmatism and defocus) and other effects (image blurring attributable to specimen movements and specimen charging; beam-induced specimen damage; etc). Consequently, these images must be digitized at a step size of 25 μm or finer and analyzed with computer-processing procedures to produce high signal-to-noise averaged images and ultimately to reconstruct a 3D density distribution ('map') of the specimen structure.

Notwithstanding the inherent complexities of preparing, imaging, and analyzing unstained specimens, the number of different macromolecules now being studied using this technology has dramatically increased in recent years. This burst of activity can be traced to the realization that with cryo-EM techniques: the details of the *entire* macromolecular structure are accessible, and not just those *surfaces* in contact with stain; the preservation of 3D structure is excellent and, for most specimens, probably extends to atomic resolution; and conformational changes, time-dependent events, and environmental influences on structure are all accessible using this technique.

In practice, high-resolution (<4 Å) 3D density maps have only been determined for a limited number of highly ordered membrane proteins (e.g. [18,19]). Even some helical structures have yielded approximately 10 Å resolution in cryoEM studies (e.g. [20–23]), clearly indicating that dedicated efforts are likely to extend these as well as other classes of molecules, including asymmetric particles such as the ribosome, to much higher resolutions.

High-resolution structural information provided by X-ray crystallography and NMR spectroscopy is seldom questioned. The validity of structural details revealed by TEM, and especially cryoTEM, is rapidly improving as the numbers of macromolecular structures being studied with both X-ray diffraction and electron microscopy increases.

Figure 1



Electron density distributions of Flock House virus displayed as surface-shaded images for the cryoEM reconstruction (top row), the calculated electron density for the X-ray model (middle row) and the difference electron density map (bottom row). **(a)** A stereo pair of the surface-shaded 3D image reconstruction of FHV. The arrow indicates the direction of view in Figure 2a where two protrusions at the quasi-threefold axes are shown with the protein model. **(b)** An equatorial cut through the reconstruction shown in (a), displaying the interior RNA density. The asterisk identifies one of the 16 cavities (four out of the total 60 are seen in this cross-section), which also appears in the X-ray model. **(c)** A stereo pair of the surface-shaded, 22 Å resolution, electron-density map computed with structure factors based on the 3.0 Å resolution X-ray protein model. **(d)** An equatorial cut through the density shown in (c), which emphasizes the absence of interior RNA density in the X-ray structure and the 16 Å cavity (asterisk). **(e)** A stereo view of the surface-shaded electron density derived from a difference map in which the X-ray model density (c) was subtracted from the density of the cryoEM reconstruction (a). The map corresponds to electron density that is not accounted for by the X-ray model and is primarily attributable to RNA. Bar=100 Å.

### Validation of low-resolution structures

Theoretical considerations outlined above suggest that the electron-density distributions derived from TEM images should be high fidelity, biologically relevant representa-

tions of the mega structures imaged. Detailed comparisons of virus structures determined by both cryoTEM and X-ray crystallography have provided compelling evidence for the exceptional quality of the EM density.

The icosahedral nodavirus Flock House virus (FHV) is one example for which X-ray and EM structures have been extensively compared [24]. An initial, qualitative comparison was made by reducing the resolution of the FHV atomic model to that of the cryoTEM structure (Fig. 1). This was done by computing structure factors, based on the atomic model, to a resolution comparable with the EM density ( $\sim 20 \text{ \AA}$ ). A high temperature factor ( $B = 2000 \text{ \AA}^2$ ) was applied to the structure factors to avoid severe Fourier termination effects when the Fourier electron-density map was computed.

The similarities in the surface features of the two structures are obvious (Figs 1a,c). Comparison of the internal density of the two structures revealed even more striking similarities (Figs 1b,d). Of particular note was a small cavity ( $16 \text{ \AA}$ ) within the protein shell that appeared in both structures. The internal density of the X-ray and cryoTEM structures revealed the complimentary nature of the two types of data. Because the X-ray structure contained few data below  $18 \text{ \AA}$  resolution, it shows little density interpretable as bulk RNA and the interior of the X-ray model is empty. The EM reconstruction, which contains complete low-resolution data, clearly shows RNA density in the center of the virus. The presence of internal features (cavity and RNA) lead to a quantitative comparison of EM and X-ray structures by means of difference, electron-density analysis. The correlation coefficient between the protein shell portions of the two density maps was maximized by adjusting an overall, radial scale factor and a single scale factor equating the averaged densities of the two structures.

A difference electron-density map (Figs 1e,2) was computed with coefficients:  $(Fe^{i\alpha})_{EM} - (Fe^{i\alpha})_{X\text{-ray}}$ . With one exception, the map revealed only RNA density, indicating the near identity of the protein densities. The region within the protein shell that appeared as positive density in the difference map was consistent with density observed on the fivefold axes of the particle in the X-ray map but was not modeled or used in the X-ray-based, structure factor calculation. At comparable resolutions, the maps displayed near perfect agreement. An internal control was included in the comparison by intentionally not including the model for ordered RNA observed in the X-ray map. This corresponds to the density observed near the twofold axes of the virus, and was the highest density in the difference map. Figure 2 shows comparisons of the FHV cryoEM map and difference map with the high-resolution X-ray model. This comparison is representative of a number of similar studies, all of which have demonstrated the remarkable quality of the reconstructed EM density (e.g. [25–28,29•,30•,31,32••]).

### Atomic modeling and refinement

The docking of atomic models into EM density maps provides a means of identifying potential, intersubunit interfaces at 'pseudo-atomic' resolution [1]. Further ex-

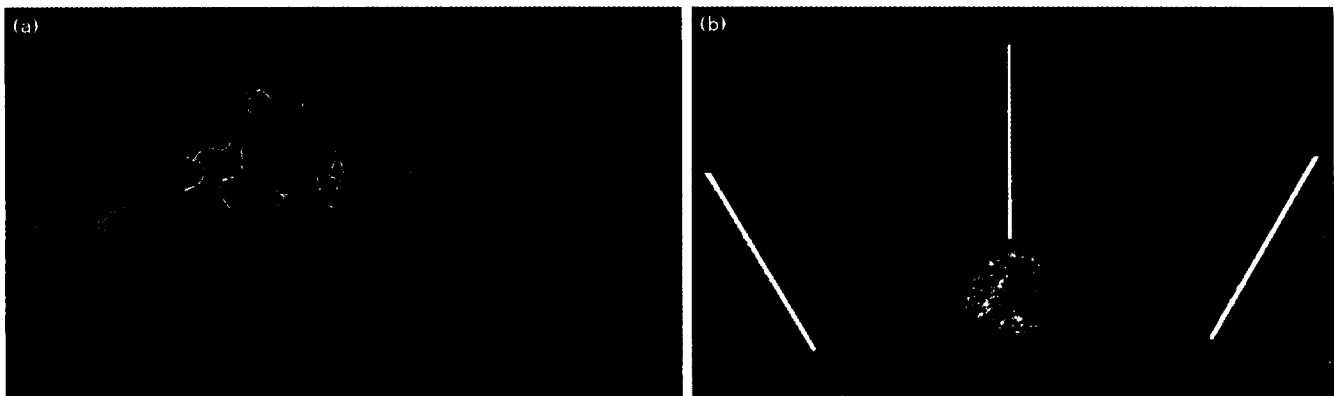
periments (e.g. mutagenesis) can be devised to test for the presence of specific interactions. The reliability of cryoEM density maps provide a firm basis for docking atomic models with a precision that exceeds by four to five times the nominal resolution of the EM data. Hence, an atomic model can be docked to within  $4\text{--}5 \text{ \AA}$  of the correct position in a  $20 \text{ \AA}$  resolution cryoEM map.

The docking results may be invalid if the molecule adopts significantly different structures in the crystal and large complex. Indeed, a reliable EM density map may be proof that a particular molecule has changed conformation (e.g. [33,34••,35••]). Ideally, molecular-fitting procedures should utilize the atomic structures of exactly those components in the complex for which the EM structure is known. An atomic model of the desired molecule is however often unavailable; the structure of a closely related molecule may be substituted with appropriate caution.

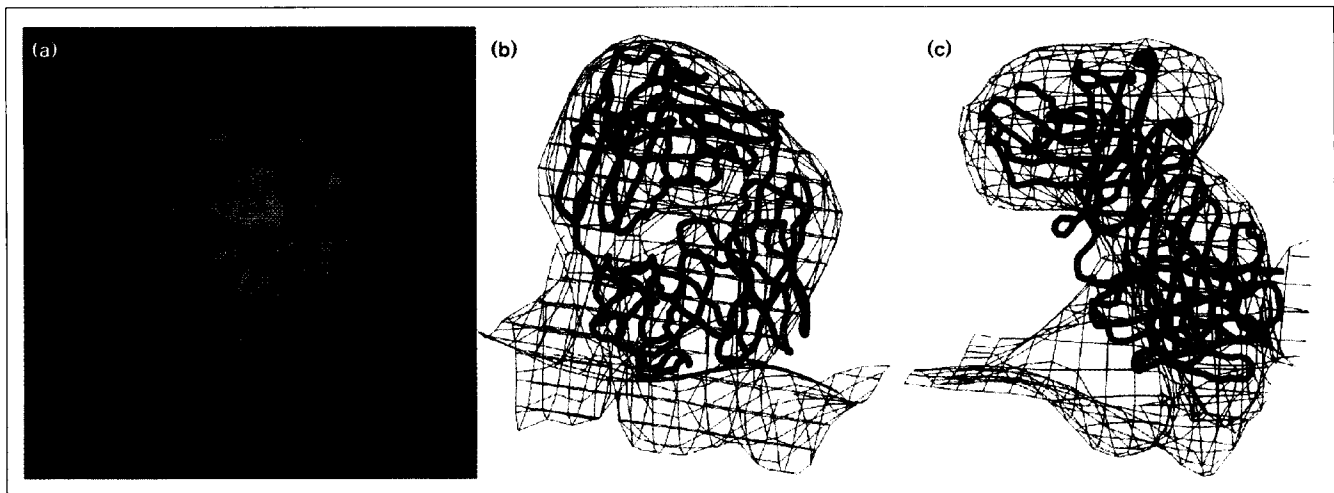
CryoTEM and 3D image reconstruction studies of antibody-mediated neutralization of viruses and the attachment of viruses to cellular receptors have benefited greatly from atomic modeling experiments (Table 1). Studies of various human rhinovirus (HRV) serotypes complexed with different neutralizing antibodies and with cellular receptor molecules illustrate clearly how atomic models of the virus and of the complexed molecules can be fitted and refined in a 3D EM density map of the complex to generate a pseudo-atomic model of the complex.

The 3D cryoTEM structure of the complex that forms when saturating amounts of a neutralizing-antibody, Fab fragment (Fab-17IA) are mixed with HRV14 was solved to  $\sim 25 \text{ \AA}$  resolution [36]. In this study, the high resolution crystal structures of both the whole virus [37] and of Fab-17IA [38] were known. The 3D reconstruction served as a constraint for docking of the Fab atomic model onto the surface of HRV. The icosahedral symmetry of the virus in the X-ray map and of the virus–Fab complex in the cryoTEM map coincided, thus fixing the absolute position and orientation of both structures. The scale (magnification) of the EM map was adjusted to match best a  $25 \text{ \AA}$  version of the X-ray map (by maximizing the cross-correlation of scaled EM maps to the HRV capsid X-ray structure). The two maps corresponded even better after the EM map had been corrected for the effects of the microscope contrast transfer function (CTF) [24]. The CTF-corrected HRV14/Fab-17IA density map also permitted more precise docking of the Fab atomic model into the EM density. Furthermore, the HRV X-ray model provided a constraint for defining the appropriate contour level to display the EM density map for the docking procedure.

The resolution of the HRV14/Fab-17IA density map was sufficient to permit accurate visual docking of the Fab-17IA atomic model as a rigid body into the

**Figure 2**

**(a)** An enlarged view of the cryoEM electron density (Fig. 1a), shown as blue contours, and the FHV X-ray model, shown as a ribbon drawing, for twofold-related prominent protrusions that are located at the quasi-threefold axes on the FHV surface. The corresponding features and the direction of view are indicated by an arrow in Figure 1a. Three polypeptide loops (16 amino acid residues each) compose each protruding feature. The fidelity of the cryoEM and X-ray structures in this region is representative of the overall consistency of the two data sets. **(b)** A cross-section view of the fit of the FHV protein C $\alpha$  atomic coordinates (yellow) into the cryoEM electron density of the full virion (blue). The contoured difference electron-density map (red lines) is superimposed on the full virion map. The locally ordered RNA, modeled as a space-filling polyribonucleotide, fits extremely well into the prominent high-radius region of the difference density at the icosahedral twofold axes, confirming the fidelity of the difference map. Icosahedral twofold and fivefold axes are depicted as white lines marked with a red ellipse and red pentagons, respectively.

**Figure 3**

Fit of Fab17-IA X-ray structure into the 3D density map reconstructed from cryoEM images of the HRV14–Fab17-IA complex. **(a)** 3D reconstruction of the virus–Fab complex viewed along a twofold axis of symmetry. The virus is depicted in shades of grey; fabs are in blue, and five-, three-, and twofold icosahedral axes of symmetry are labeled. **(b)** Magnified view of the Fab17-IA X-ray structure (C $\alpha$  backbone of the Fab heavy chain is red; C $\alpha$  backbone of the Fab light chain is blue) fitted into the cryoEM electron-density envelope (black lines). The view direction is approximately from a fivefold axis of the virus towards a twofold axis. The variable domain of the Fab is toward the bottom. **(c)** Same as middle panel except that the view direction is rotated 90° about the vertical direction.

corresponding Fab envelope (Fig. 3). Translations of the Fab model by as little as 2–4 Å from the visual fit moved large portions of the model outside the EM envelope or caused the two models to overlap. Though quantitative docking of Fab 17-IA gave no substantial improvement of the fit to the HRV14/Fab-17IA map, such procedures

can be helpful when the EM envelope lacks asymmetric features or does not contain sufficient detail (e.g. [39\*]).

The docking procedure leads to a pseudo-atomic model of the complex, from which interacting interfaces ('the footprint') between the Fab and virus surface can be

defined and the reasonableness of the interface can be examined. On this basis, a number of complementary, electrostatic interactions in the HRV–Fab complex were recognized as contributing to the binding affinity of the Fab for the virus. Mutagenesis experiments confirmed the importance of such interactions [38].

The study of the binding of the cellular receptor molecule intercellular adhesion molecule (ICAM)-1, to the major group of rhinoviruses [40,41], represents the more typical example of an atomic modeling experiment. A cryoTEM reconstruction of the HRV16/ICAM-1 complex was computed. Atomic models for HRV16 and ICAM-1 were not available so X-ray models of HRV14 and CD4 (the HIV-1 receptor) were used as substitute structures for docking experiments [40]. The receptor molecule binds into a depression on the virus referred to as the ‘canyon’ in a manner quite similar to that proposed years earlier [37]. It was, however, considered inappropriate to extend this qualitative analysis and attempt to define detailed molecular interactions between ICAM and HRV. Similar caution may be appropriate when attempts are made to interpret pseudo-atomic models derived from an EM density map of a macromolecular complex that lacks one or more of the modeled components (e.g. [42,43,44\*,45\*\*]).

### Low resolution leads to high

A significant development in modern molecular and structural biology has been the ability to crystallize large, complicated structures such as the ribosome [46] or antibody–virus complexes [47]. These crystals will lead to high-resolution structures that will require only limited modeling and interpretation to establish authentic complex structures. The phase problem for such structures may be daunting, particularly when the non-crystallographic symmetry is limited as in the ribosome. It is likely that the hybrid atomic resolution models discussed above will play a pivotal role in phasing such complexes. Carefully collected, low-resolution crystallographic data, together with sophisticated, moderate-resolution models, should provide a molecular-replacement phase solution at low resolution. Such a solution will probably make possible the determination of heavy-atom sites that can then be used for multiple, isomorphous-replacement phase determination. In the case of symmetric particles such as viruses, even crude initial models can be adequate to allow direct extension of phases to high resolution with the use of non-crystallographic symmetry-averaging (e.g. [48,49]).

### Conclusion

Only a few years ago it was not clear how a continuum in resolution of biological structures could be achieved. The superb light microscopy of cellular biology merged smoothly with cytological electron microscopy but a distinct gap was evident between these studies and those of molecular EM, X-ray crystallography, and NMR spectroscopy. It is now apparent that a way exists of

bridging this gulf, with the long-term goal of providing a ‘zoom lens’ for visualizing biological structures from cells to atoms. The major obstacle that currently limits the use of this method is the production of soluble, crystallizable forms of the individual proteins comprising the megastructures. Because they are designed to make homo- or heteromeric associations, they are generally, at best, marginally soluble in the isolated, non-denatured form. Because this property may result from a limited number of residues on the protein surface, a genetic approach for the introduction of random, single or limited site mutations into the component protein gene, coupled with an assay for the solubility of the expressed protein, is needed to render the approach generally applicable.

### Acknowledgements

Work in the authors’ laboratories discussed in this paper was supported by National Institutes of Health grants GM-33050 (TSB) and GM34220 (JEJ). We thank Norm Olson for insightful comments on the manuscript, and Tom Smith for providing Figure 3 and for his continued inspiration and ideas.

### References and recommended reading

Papers of particular interest, published within the annual period of review, have been highlighted as:

- of special interest
  - of outstanding interest
1. Hogle JM: **The viral canyon.** *Curr Biol* 1993, **3**:278–281.
  2. Chiu W, Smith TJ: **Structural studies of virus-antibody complexes by electron cryomicroscopy and X-ray crystallography.** *Curr Biol* 1994, **4**:219–224.
  3. Stewart PL, Burnett RM: **Spherical virus assembly.** *Curr Opin Struct Biol* 1994, **4**:213–218.
  4. Smith TJ, Mosser AG, Baker TS: **Structural studies on the mechanisms of antibody-mediated neutralization of human rhinovirus.** *Semin Virol* 1995, **6**:233–242.
  5. Johnson JE: **Functional implications of protein–protein interactions in icosahedral viruses.** *Proc Natl Acad Sci USA* 1996, **93**:27–33.
  6. Reedy MK: **Myosin–actin motors: the partnership goes atomic.** *Structure* 1993, **1**:1–5.
  7. Rayment I, Holden HM: **The three-dimensional structure of a molecular motor.** *Trends Biochem Sci* 1994, **19**:129–134.
  8. Egelman EH, Orlova A: **New insights into actin filament dynamics.** *Curr Opin Struct Biol* 1995, **5**:172–180.
  9. Milligan RA: **Protein–protein interactions in the rigor actomyosin complex.** *Proc Natl Acad Sci USA* 1996, **93**:21–26.
  10. Chiu W: **What does electron cryomicroscopy provide that X-ray crystallography and NMR spectroscopy cannot?** *Annu Rev Biophys Biomol Struct* 1993, **22**:233–255.
  11. Holmes KC: **Solving the structures of macromolecular complexes.** *Structure* 1994, **2**:589–593.
  12. Thomas JM: **Architecture of the invisible.** *Nature* 1994, **364**:478–482.
  13. Henderson R, Unwin PNT: **Three-dimensional model of purple membrane obtained by electron microscopy.** *Nature* 1975, **257**:28–32.
  14. Taylor KA: **Structure determination of frozen, hydrated, crystalline biological specimens.** *J Microsc* 1978, **112**:115–125.
  15. Milligan RA, Brisson A, Unwin PNT: **Molecular structure determination of crystalline specimens in frozen aqueous solutions.** *Ultramicroscopy* 1984, **13**:1–10.
  16. Stewart M, Vigers G: **Electron microscopy of frozen-hydrated biological material.** *Nature* 1986, **319**:631–636.

17. Dubochet J, Adrian M, Chang JJ, Homo JC, Lepault J, McDowell AW, Schultz P: **Cryo-electron microscopy of vitrified specimens.** *Q Rev Biophys* 1988, **21**:129–228.
18. Henderson R, Baldwin JM, Ceska TA, Zemlin F, Beckmann E, Downing KH: **Model for the structure of bacteriorhodopsin based on high-resolution electron cryo-microscopy.** *J Mol Biol* 1990, **213**:899–929.
19. Kühlbrandt W, Wang DN, Fujiyoshi Y: **Atomic model of plant light-harvesting complex by electron crystallography.** *Nature* 1994, **367**:614–621.
20. Jeng TW, Crowther RA, Stubbs G, Chui W: **Visualization of  $\alpha$ -helices in tobacco mosaic virus by cryo-electron microscopy.** *J Mol Biol* 1989, **205**:251–257.
21. Morgan DG, Owen C, Melanson LA, DeRosier DJ: **Structure of bacterial flagellar filaments at 11 Å resolution: packing of the  $\alpha$ -helices.** *J Mol Biol* 1995, **249**:88–110.
22. Mimori Y, Yamashita I, Murata K, Fujiyoshi Y, Yonekura K, Toyoshima C, Namba K: **The structure of the R-type straight flagellar filament of *Salmonella* at 9 Å resolution by electron cryomicroscopy.** *J Mol Biol* 1995, **249**:69–87.
23. Unwin N: **Acetylcholine receptor channel imaged in the open state.** *Nature* 1995, **373**:37–43.
24. Cheng RH, Reddy V, Olson NH, Fisher A, Baker TS, Johnson JE: **Functional implications of quasi-equivalence in a T=3 icosahedral animal virus established by cryo-electron microscopy and x-ray crystallography.** *Structure* 1994, **2**:271–282.
25. Stewart PL, Fuller SD, Burnett RM: **Difference imaging of adenovirus: bridging the resolution gap between X-ray crystallography and electron microscopy.** *EMBO J* 1993, **12**:2589–2599.
26. Wang G, Porta C, Chen Z, Baker TS, Johnson JE: **Identification of a  $F_{ab}$  interaction site (footprint) on an icosahedral virus by cryo-electron microscopy and x-ray crystallography.** *Nature* 1992, **355**:275–278.
27. Wikoff WR, Wang G, Parrish CR, Cheng RH, Strassheim ML, Baker TS, Rossmann MG: **Structures of a neutralized virus: canine parvovirus complexed with neutralizing antibody fragments.** *Structure* 1994, **2**:595–607.
28. Voges D, Berendes R, Burger A, Demange P, Baumeister W, Huber R: **Three-dimensional structure of membrane-bound annexin V: a correlative electron microscopy-X-ray crystallographic study.** *J Mol Biol* 1994, **238**:199–213.
29. Ilag LL, Olson NH, Dokland T, Music CL, Cheng RH, Bowen Z, McKenna R, Rossmann MG, Baker TS, Incardona NL: **DNA packaging intermediates of bacteriophage  $\phi$ X174.** *Structure* 1995, **3**:353–363.
- Modeling of the atomic structures of the F and G virion proteins (from the crystal structure of the 70S virion) into cryoEM reconstructions of 108S procapsids and 132S provirions shows that the G and F proteins undergo minor and major conformational changes, respectively; these changes are believed to help facilitate viral assembly.
30. Speir JA, Munshi S, Wang G, Baker TS, Johnson JE: **Structures of the native and swollen forms of cowpea chlorotic mottle virus determined by x-ray crystallography and cryo-electron microscopy.** *Structure* 1995, **3**:63–78.
- The 3.2 Å structure of the native virus is determined by X-ray crystallography. The atomic-resolution subunit model is then fitted to the cryoEM density for a swollen form of the virus, demonstrating that electrostatic repulsion from ionized acidic residues causes the swelling at neutral pH in the absence of divalent metal ions.
31. Baker TS, Cheng RH: **A model-based approach for determining orientations of biological macromolecules imaged by cryo-electron microscopy.** *J Struct Biol* 1996, **116**:120–130.
32. Avila-Saker AJ, Chiu W: **Visualization of  $\beta$ -sheets and side-chain clusters in two-dimensional periodic arrays of streptavidin on phospholipid monolayers by electron crystallography.** *Biophys J* 1996, **70**:57–68.
- Two dimensional crystals of streptavidin are ordered to 2.5 Å resolution. Electron-diffraction data are collected and used for the refinement of the available X-ray atomic model using the program X-PLOR. An agreement factor of 18% is obtained while maintaining good geometry in the protein. The coordinates of the model refined against the electron diffraction data are closely similar to the X-ray coordinates.
33. Smith TJ, Olson NH, Cheng RH, Chase ES, Baker TS: **Structure of a human rhinovirus-bivalently bound antibody complex: implications for virus neutralization and antibody flexibility.** *Proc Natl Acad Sci USA* 1993, **90**:7015–7018.
34. Jontes JD, Wilson-Kubalek EM, Milligan RA: **A 35-Å tail swing in brush border myosin I on ADP release.** *Nature* 1995, **378**:751–753.
- Cryo-EM and image analysis reveal conformational changes in brush border myosin I-decorated actin in response to Mg-ADP. The conformational changes are larger than those seen in smooth muscle myosin [35\*\*]. Docking of the homologous region of the X-ray structure of skeletal S1 (the motor domain) into the EM maps demonstrates that even a limited amount of high-resolution information can provide insight into the nature of the changes: the light-chain region rotates as a rigid body about its junction with the immobile motor domain.
35. Whittaker M, Wilson-Kubalek EM, Smith JE, Faust L, Milligan RA, Sweeney HL: **A 35-Å movement of smooth muscle myosin on ADP release.** *Nature* 1995, **378**:748–751.
- The combination of low-resolution EM maps of smooth-muscle-S1-decorated actin in two distinct conformational states ( $\pm$ Mg-ADP) with the X-ray structure of the myosin head allows interpretation of the structural changes in terms of a rigid-body rotation of only the myosin-light-chain-containing region of the molecule. Together with the results in [34\*\*], these data represent the first direct demonstration that the myosin head changes conformation when it is attached to actin.
36. Smith TJ, Olson NH, Cheng RH, Liu H, Chase ES, Lee WM, Leippe DM, Mosser AG, Rueckert RR, Baker TS: **Structure of human rhinovirus complexed with  $F_{ab}$  fragments from a neutralizing antibody.** *J Virol* 1993, **67**:1148–1158.
37. Rossmann MG, Arnold E, Erickson JW, Frankenberger EA, Griffith JP, Hecht HJ, Johnson JE, Kamer G, Luo M, Mosser AG *et al.*: **Structure of a human common cold virus and functional relationship to other picornaviruses.** *Nature* 1985, **317**:145–153.
38. Liu H, Smith TJ, Lee WM, Mosser AG, Rueckert RR, Olson NH, Cheng RH, Baker TS: **The purification, crystallization and structure determination of an  $F_{ab}$  fragment that neutralizes human rhinovirus 14 and analysis of the  $F_{ab}$ -virus complex.** *J Mol Biol* 1994, **240**:127–137.
39. Cheng RH, Kuhn RJ, Olson NH, Rossmann MG, Choi HK, Smith TJ, Baker TS: **Three-dimensional structure of an enveloped alphavirus with T=4 icosahedral symmetry.** *Cell* 1995, **80**:621–630.
- Modeling of atomic structure of the Sindbis core protein into the cryoEM reconstruction of the nucleocapsid portion of Ross River virus shows that the nucleocapsid protein does not associate as dimers, as predicted on the basis of crystallographic experiments. Instead, the capsid proteins are arranged as pentamers and hexamers in a T=4 lattice and in one-to-one association with the 240 E1:E2 glycoprotein heterodimers.
40. Olson NH, Kolatkar PR, Oliveria MA, Cheng RH, Greve JM, McClelland A, Baker TS, Rossmann MG: **Structure of a human rhinovirus complexed with its receptor molecule.** *Proc Natl Acad Sci USA* 1993, **90**:507–511.
41. Rossmann MG: **Viral cell recognition and entry.** *Protein Sci* 1994, **3**:1712–1725.
42. Frank J, Zhu J, Penczek P, Li Y, Srivastava S, Verschoor A, Radermacher M, Grassucci R, Lata RK, Agrawal RK: **A model of protein synthesis based on cryo-electron microscopy of the *E. coli* ribosome.** *Nature* 1995, **376**:441–444.
43. Frank J, Verschoor A, Li Y, Zhu J, Lata RK, Radermacher M, Penczek P, Grassucci R, Agrawal RK, Srivastava S: **A model of the translational apparatus based on a three-dimensional reconstruction of the *Escherichia coli* ribosome.** *Biochem Cell Biol* 1995, **73**:757–765.
44. Stark H, Mueller F, Orlova EV, Schatz M, Dubel P, Erdemir T, Zemlin F, Brimacombe R, Van Heel M: **The 70S *Escherichia coli* ribosome at 23 Å resolution: fitting the ribosomal RNA.** *Structure* 1995, **3**:815–821.
- The authors describe the preliminary fitting of the double-helical regions of a rRNA, from a 3D model based on biochemical data, to a cryoEM reconstruction of the 70S ribosome. The reconstruction shows an extensive system of channels within the 50S subunit and a gap between the 30S and 50S subunits, reported to be ideally shaped to accommodate two tRNA molecules.
45. Agrawal RK, Penczek P, Grassucci RA, Li Y, Leith A, Nierhaus K, Frank J: **Direct visualization of A-, P-, and E-site transfer RNAs in the *Escherichia coli* ribosome.** *Science* 1996, **271**:1000–1002.
- This paper reports the atomic modelling of tRNA molecules into a difference density map computed between maps of the native 70S ribosome and of a poly(U) programmed 70S ribosome in which the sites were occupied by three deacylated tRNA<sup>Phe</sup> molecules. The results help identify the locations

of the sites for anticodon interaction and peptide bond formation on the ribosome. Note how these results compare with those reported in [42,43,44\*].

46. Berkovitch-Yellin Z, Bennet WS, Yonath A: **Aspects in structural studies on ribosomes.** *Crit Rev Biochem Mol Biol* 1992, **27**:403–444.
47. Smith TJ, Chase ES: **Purification and crystallization of intact human rhinovirus complexed with a neutralizing Fab.** *Virology* 1993, **191**:600–606.
48. Rayment I, Baker TS, Caspar DLD, Murakami WR: **Polyoma virus capsid crystal structure at 22.5 Å resolution.** *Nature* 1982, **295**:110–115.
49. Rayment I, Baker TS, Caspar DLD: **A description of the techniques and application of molecular replacement used to determine the structure of polyoma virus capsids at 22.5 Å resolution.** *Acta Crystallogr [B]* 1983, **39**:505–516.
50. Saibil HR: **How chaperones tell wrong from right.** *Nat Struct Biol* 1994, **1**:838–842.
51. Harris JR, Holzenburg A: **Human erythrocyte catalase: 2-D crystal nucleation and production of multiple crystal forms.** *J Struct Biol* 1995, **115**:102–112.
52. Dabrowski JJ, Yanchunas J Jr, Villafranca BC, Dietze EC, Schurke P, Atkins WM: **Supramolecular self-assembly of glutamine synthetase: mutagenesis of a novel intermolecular metal binding site required for dodecamer stacking.** *Biochemistry* 1994, **33**:14957–14964.
53. Celia H, Hoermann L, Schultz P, Lebeau L, Mallouh V, Wigle DB, Wang JC, Mioskowski C, Oudet P: **Three-dimensional model of *Escherichia coli* gyrase B subunit crystallized in two-dimensions on novobiocin-linked phospholipid films.** *J Mol Biol* 1994, **236**:618–628.
54. Kubalek EW, LeGrice SFJ, Brown PO: **Two-dimensional crystallization of histidine-tagged, HIV-1 reverse transcriptase promoted by a novel nickel-chelating lipid.** *J Struct Biol* 1994, **113**:117–123.
55. Newman RH, Carpenter E, Freemont PS, Blundell TL, Parker PJ: **Microcrystals of the beta 1 isoenzyme of protein kinase C: an electron microscopic study.** *Biochem J* 1994, **298**:391–393.
56. Demange P, Voges D, Benz J, Liemann S, Göttig P, Benendes R, Burger A, Huber R: **Annexin V: the key to understanding ion selectivity and voltage regulation?** *Trends Biochem Sci* 1994, **19**:272–276.
57. Kamikubo H, Kataika M, Varo G, Oka T, Tokunaga F, Needleman R, Lanyi JK: **Structure of the N intermediate of bacteriorhodopsin revealed by x-ray diffraction.** *Proc Natl Acad Sci USA* 1996, **93**:1386–1390.
58. Cabral-Lilly D, Sosinsky GE, Reed RA, McDermott MR, Shipley GG: **Orientation of cholera toxin bound to model membranes.** *Biophys J* 1994, **66**:935–941.
59. Capaldi RA: **F<sub>1</sub>-ATPase in a spin.** *Nat Struct Biol* 1994, **1**:660–663.
60. Bullough PA, Hughson FM, Skehel JJ, Wiley DC: **Structure of influenza haemagglutinin at the pH of membrane fusion.** *Nature* 1994, **371**:37–43.
61. Wharton SA, Calder LJ, Ruigrok RW, Skehel JJ, Steinhauer DA, Wiley DC: **Electron microscopy of antibody complexes of influenza virus haemagglutinin in the fusion pH conformation.** *EMBO J* 1995, **14**:240–246.
62. Savage H, Cyrklaff M, Montoya G, Kühlbrandt W, Sinning I: **Two-dimensional structure of light harvesting complex II (LHII) from the purple bacterium *Rhodovulum sulfidophilum* and comparison with LHII from *Rhodospseudomonas acidophila*.** *Structure* 1996, **4**:243–252.

The two dimensional structure of LH(II) from *Rhodovulum sulfidophilum* is determined at 7 Å resolution by cryoEM. The structure is compared with the 2.5 Å resolution atomic model of LH(II) from *Rhodospseudomonas acidophila*. The two structures correlate very well with the major difference being a slight displacement of the outer helices, perhaps attributable to a different degree of tilt in these helices in the two structures.

63. Schabert FA, Henn C, Engel A: **Native *Escherichia coli* OmpF porin surfaces probed by atomic force microscopy.** *Science* 1995, **268**:92–94.

Atomic models of protein-protein and lipid-protein interactions are developed on the basis of the X-ray crystal structure of the OmpF porin trimer and topographs recorded by atomic force microscopy (AFM) of 2D crystals reconstituted in the presence of lipids. The bilayer is modeled with kinked

lipids by fitting the head groups to contours determined with AFM. The potential of AFM to monitor conformational changes at high resolution is clearly demonstrated.

64. Boekema EJ, Hankamer B, Bald D, Kruijff J, Nield J, Boonstra AF, Barber J, Rogner M: **Supramolecular structure of the photosystem II complex from green plants and cyanobacteria.** *Proc Natl Acad Sci USA* 1995, **92**:175–179.
65. Parker MW, Buckley JT, Postma JP, Tucker AD, Leonard K, Pattus F, Tsernoglou D: **Structure of the *Aeromonas* toxin proaerolysin in its water-soluble and membrane-channel states.** *Nature* 1994, **367**:292–295.
66. Czarnota GJ, Andrews DW, Farrow NA, Ottensmeyer FP: **A structure for the signal sequence binding protein SRP54: 3D reconstruction from STEM images of single molecules.** *J Struct Biol* 1994, **113**:35–46.
67. Schmidt MF, Jakana J, Matsudaira P, Chiu W: **Three-dimensional structure of the acrosomal filament of *Limulus* sperm by 400 kV electron cryomicroscopy.** *Biophys J* 1995, **68**:8S–11S.

The chemical basis for straightening the acrosomal process in the fertilization reaction of *Limulus* sperm is examined. An acrosomal bundle formed of an actin filament with associated scruin molecules is imaged at 7 Å resolution using cryoEM and image processing. Fitting the atomic model of F-actin to the EM map allows the identification of residues on actin that interact with scruin.

68. Schmid MF, Agris JM, Jakana J, Matsudaira P, Chiu W: **Three-dimensional structure of a single filament in the *Limulus* acrosomal bundle: scruin binds to homologous helix-loop-beta motifs in actin.** *J Cell Biol* 1994, **124**:341–350.
  69. Schmid MF, Jakana J, Chiu W: **A 7-Å projection map of frozen, hydrated acrosomal bundle from *Limulus* sperm.** *J Struct Biol* 1995, **115**:209–213.
  70. Mendelson R, Morris E: **Combining electron microscopy and X-ray crystallography data to study the structure of F-actin and its implications for thin-filament regulation in muscle.** *Adv Exp Med Biol* 1994, **358**:13–23.
  71. Mendelson R, Morris E: **The structure of F-actin. Results of global searches using data from electron microscopy and X-ray crystallography.** *J Mol Biol* 1994, **240**:138–154.
  72. Orlova A, Egelman EH: **Structural dynamics of F-actin: I. Changes in the C terminus.** *J Mol Biol* 1995, **245**:582–597.
  73. Orlova A, Prochniewicz E, Egelman EH: **Structural dynamics of F-actin: II. Cooperativity in structural transitions.** *J Mol Biol* 1995, **245**:598–607.
  74. McGough A, Way M, DeRosier D: **Determination of the  $\alpha$ -actinin-binding site on actin filaments by cryoelectron microscopy and image analysis.** *J Cell Biol* 1994, **126**:433–443.
  75. McGough A, Way M: **Molecular model of an actin filament capped by a severing protein.** *J Struct Biol* 1995, **115**:144–150.
  76. Lehman W, Vibert P, Uman P, Craig R: **Steric-blocking by tropomyosin visualized in relaxed vertebrate muscle thin filaments.** *J Mol Biol* 1995, **251**:191–196.
- An atomic resolution model of F-actin is fitted to the negative-stain, EM-derived, density of skeletal muscle filaments. A cleft in the F-actin model agrees well with a complementary feature in the EM map, supporting the fit. The fit of the high-resolution model supports the mechanism by which strong cross-bridge association between actin and myosin is inhibited in relaxed muscle by a troponin-stabilized form of tropomyosin.
77. Orlova A, Yu X, Egelman EH: **Three-dimensional reconstruction of a co-complex of F-actin with antibody fragments to actin's NH<sub>2</sub> terminus.** *Biophys J* 1994, **66**:276–285.
  78. Padrón R, Alamo L, Guerrero JR, Granados M: **Three-dimensional reconstruction of thick filaments from rapidly frozen, freeze-substituted tarantula muscle.** *J Struct Biol* 1995, **115**:250–257.
  79. Holmes KC: **The actomyosin interaction and its control by tropomyosin.** *Biophys J* 1995, **68**:2S–7S.
  80. Xie X, Rao S, Walian P, Hatch V, Phillips GN Jr, Cohen C: **Coiled-coil packing in spermine-induced tropomyosin crystals: a comparative study of three forms.** *J Mol Biol* 1994, **236**:1212–1226.
  81. DeHaas F, VanBruggen EF: **The interhexameric contacts in the four-hexameric hemocyanin from the tarantula *Eurypelma californicum*. A tentative mechanism for cooperative behavior.** *J Mol Biol* 1994, **237**:464–478.
  82. VanHeel M, Dube P: **Quaternary structure of multihexameric arthropod hemocyanins.** *Micron* 1994, **25**:387–418.

83. DeHaas F, Pertou FG, VanBremen JF, Dijkema JH, Beintema JJ, VanBruggen EF: **Identification of two antibody-interaction sites on the surface of *Panulirus interruptus* hemocyanin.** *Eur J Biochem* 1994, **222**:155–161.
84. Boisset N, Penczek P, Taveau JC, Lamy J, Frank J, Lamy J:  
 • **Three-dimensional reconstruction of *Androctonus australis* hemocyanin labeled with a monoclonal Fab fragment.** *J Struct Biol* 1995, **115**:16–29.
- The 3D fitting of closely related X-ray structures of *Panulirus interruptus* hemocyanin and of Fab R19.9 to the cryoEM reconstruction of the scorpion 4 x 6meric hemocyanin–Fab L104 complex localized the epitope to the surface of the Aa6 hemocyanin subunit.
85. Moore PB: **Ribosomes seen through a glass less darkly.** *Structure* 1995, **3**:851–852.
86. Smith TJ, Cheng RH, Olson NH, Peterson P, Chase E, Kuhn RJ,  
 • Baker TS: **Putative receptor binding sites on enveloped viruses as visualized by cryo-electron microscopy.** *Proc Natl Acad Sci USA* 1995, **92**:10648–10652.
- Modelling of Fab atomic structures into cryoEM reconstructions of Sindbis Fab and Ross River-Fab complexes shows that the two monoclonal antibodies bind in slightly different orientations to identical locations on the E2 glycoproteins. These constitute the putative receptor binding sites for both viruses.
87. Porta C, Wang G, Cheng RH, Chen Z, Baker TS, Johnson JE:  
**Direct imaging of interactions between an icosahedral virus and conjugate F<sub>ab</sub> fragments by cryo-electron microscopy and x-ray crystallography.** *Virology* 1994, **204**:777–788.
88. Baker TS, Johnson JE: **Principles of virus structure determination.** In *Structural Biology of Viruses*. Edited by Chiu W, Burnett RM, Garcea R. New York: Oxford University Press; 1996: in press.
89. Rossmann MG, Olson NH, Kolatkar PR, Oliverira MA, Cheng RH, Greve JM, McClelland A, Baker TS: **Crystallographic and cryo EM analysis of virion-receptor interactions.** *Arch Virol Suppl* 1994, **9**:531–541.
90. Hewat EA, Blaas D: **Structure of a neutralizing antibody bound bivalently to human rhinovirus 2.** *EMBO J* 1996, **15**:1515–1523.

CryoEM and atomic modelling study of the complex formed between a minor-group rhinovirus (HRV2) and a weakly neutralizing, monoclonal IgG demonstrates bivalent attachment of the antibody. This study compares and contrasts with similar work on complexes formed between strongly neutralizing antibodies and the major-group rhinovirus (HRV14) [4,33,36,38,91\*\*,92].

91. Smith TJ, Chase ES, Schmidt TJ, Olson NH, Baker TS:  
 •• **Neutralizing antibody to human rhinovirus 14 penetrates the receptor-binding canyon.** *Nature* 1996, in press.
- The first moderate resolution (4 Å) crystal structure of a virus–Fab complex reveals details of Fab–virus interactions. The pseudo-atomic model of HRV14–Fab 171A [36,38] served as an initial phasing model for the X-ray crystallographic structure determination.
92. Smith TJ, Olson NH, Che Z, Chase E, Cheng RH, Baker TS, Mosser AG, Leippe D, Rueckert RR: **Structural studies on virus-antibody interactions.** In *Vaccines96: Molecular Approaches to the Control of Infectious Diseases*. Edited by Brown F, Norrby E, Burton D, Mekalanos J. Cold Spring Harbor: Cold Spring Harbor Laboratory Press; 1996:161–167.
93. Chipman PR, Agbandje-McKenna M, Kajigaya S, Brown KE, Young NS, Baker TS, Rossmann MG: **Cryo-electron microscopy studies of empty capsids of human parvovirus B19, complexed with its cellular receptor.** *Proc Natl Acad Sci USA* 1996, **93**:7502–7506.
- The second cryoEM reconstruction of a virus–receptor complex (compare with [40]). The glycolipid receptor molecules bind into depressions on the threefold axes of the B19–globoside complex. An atomic model of the tetrasaccharide component of the globoside receptor fits nicely into a difference map of the globoside density.
94. Grimes J, Basak AK, Roy P, Stuart D: **The crystal structure of bluetongue virus VP7.** *Nature* 1995, **343**:167–170.
- The 2.6 Å resolution structure of the VP7 subunit (349 amino acids) of blue tongue virus is determined by X-ray crystallography. A pseudo-atomic resolution model of the T=13 (780 subunits, 700 Å diameter) core of the virus is constructed by fitting the VP7 X-ray model to the 35 Å structure of the core, determined previously by cryoEM and image reconstruction.
95. Beroukhir R, Unwin N: **Three-dimensional location of the main immunogenic region of the acetylcholine receptor.** *Neuron* 1995, **15**:323–331.